BULLETIN OF THE POLISH ACADEMY OF SCIENCES
TECHNICAL SCIENCES, Vol. 70(1), 2022, Article number: e139957
DOI: 10.24425/bpasts.2021.139957

Tuning PID and PI-PI servo controllers by multiple pole placement

Andrzej BOŻEK* and **Leszek TRYBUS**

Department of Computer and Control Engineering, Rzeszów University of Technology, W. Pola 2, 35-959 Rzeszów, Poland

Abstract. Tuning rules for PID and PI-PI servo controllers are developed using a pole placement approach with a multiple pole, i.e. a triple one in the case of PID and a quadruple for PI-PI. The controllers involve complex roots in the numerators of the transfer functions. This is not possible in the classical P-PI structure which admits real roots only. The settling time of the servos determined by the multiple time constant is the only design parameter. Nomograms to read out discrete controller settings in terms of the time constant and control cycle are given. As compared to the classical structures, the upper limit on the control cycle is now twice longer in the case of PID, and four times in the case of PI-PI. This implies that the settling times can be shortened by the same ratios. Responses of a PLC-controlled servo confirm the validity of the design.

Key words: servomechanism; double integrator; pole placement; PID controller; discrete-time control.

1. INTRODUCTION

Servomechanisms, called servos for short, as motion control systems are final execution elements of robots, machine tools, conveyors, etc. [1]. Extensive analyses, design solutions, and applications of the servos are described in [2, 3]. Robot servos are typically equipped with permanent magnet (PM) brushless DC (BLDC) motors or AC synchronous motors (PMSM) driven by suitable power devices. A classical control structure involves a torque controller (two-axis controllers for PMSM), a PI velocity loop, and an outer P position loop. This P-PI setup is equivalent to a single PID with real roots (zeros) in the transfer function numerator. By neglecting viscous friction, a servomotor equipped with a torque controller is typically described by a double integrator.

The double integrator with a P-PI or PID controller is a 3rd order system expected to provide smooth responses with a prescribed settling time. Identification of electrical parameters and step-by-step tuning of current (torque), velocity, and position controllers for a PMSM servo-drive is described in [4]. Conventional frequency methods are applied for design in [2, 3], given natural frequency and damping ratio. The considerations on the application of root-locus method [5] can be found in [6]. The detailed design of a constrained state feedback controller for a PMSM servo described in [7] may be an example of advanced approaches. Assessments of PD, LQG, minimum time, sliding mode and a few other algorithms for control of the double integrator at off-normal conditions are presented in [8]. In practice, however, industrial servos are usually tuned by trial-and-error.

Fast tool servo devices, particularly direct drives, may be equipped with additional acceleration feedback loop involving an acceleration sensor and acceleration controller providing a set-point for the current controller. The idea was initially proposed in [9]. The acceleration signal represents instantaneous net reaction of the moved mass to current-generated control force and disturbance forces due to varying load, vibrations, etc. The additional loop, usually proportional, reduces the effect of disturbance forces thus enhancing the performance of the servo. For P-PI or PID position controllers a servo-drive equipped with the acceleration loop still looks like a double integrator.

Application of the root-locus method for the design of P-PI servo controller was described in this journal in [10]. The relative simplicity of the 3rd order system enabled analytic solution for a controller with double real zero. The PI-PI structure, appropriate for suppressing varying disturbances, was considered as well. Simple rules for setting controller parameters in terms of required settling time, design nomograms for discrete implementations, and limits on control cycle time were provided.

From a practical point of view it may be useful to indicate that a controller with settings obtained by continuous design requires sufficiently fast sampling what, if time requirements are high, implies the application of an embedded servo-controller or an external PLC dedicated solely to the servo. If however, the PLC executes also some other tasks, the computational load required by fast sampling may turn out unacceptable. In such a case discrete design is needed, together with knowledge of the maximum control cycle which provides the lowest computational load.

Some time ago the authors became interested in Internal Model Control (IMC) method popular in the process control community, particularly for plants with delay, e.g. [11,12]. IMC design provides smooth responses defined by a time constant λ (usually multiple) being the only design parameter. Due to such

*e-mail: abozek@prz.edu.pl

Manuscript submitted 2021-05-10, revised 2021-09-22, initially accepted for publication 2021-10-19, published in February 2022.

features, application of the IMC to servo design seemed interesting.

As it turned out the IMC solution is equivalent to pole placement (modal) with a triple pole $1/\lambda$. The resulting PID controller has complex zeros, so has to be implemented as "standalone" (Fig. 1), and not as the P-PI structure with two nested loops. By application of a quadruple pole placement, the PI-PI structure can also be considered. In the case of discrete implementations, the new design relaxes considerably the requirements on control cycle time, which may be beneficial for high-performance servos [7] or when a PLC executes other tasks in parallel.

This paper, often referring to [10], is organized as follows. The next section reviews briefly the previous root-locus design and presents a relatively uncomplicated new solution based on triple pole placement. A discrete PID controller for which the design becomes more involved is considered in Section 3. A nomogram for the selection of controller settings and upper limit on control cycle are given. Continuous and discrete PI-PI structures are dealt with in Sections 4 and 5, respectively. A lab servo set-up with responses for the control cycle corresponding to the upper limit is considered in Section 6. Continuous control is tested as well by applying the shortest control cycle available in the set-up PLC. Alternative PID design using IMC is presented in Appendix.

2. CONTINUOUS PID CONTROLLER FOR DOUBLE INTEGRATOR

We begin with a review of the design from [10].

2.1. Root-locus

Consider the control system of Fig. 1 involving a double integrator, PID controller, and reference filter F. The double integrator k_o/s^2 represents in practice a connection of servo-drive, servomotor and mechanical load resulting in the effective gain k_o.

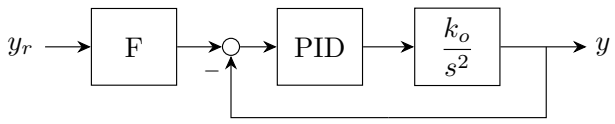

Fig. 1. PID control system for double integrator

Let the controller be described by

$$G_{\mathrm{PID}}(s) = k_P + \frac{k_I}{s} + k_D s \tag{1}$$

with the gains k_P, k_I, k_D of corresponding PID actions. As demonstrated later in Section 4, such a controller may be converted into classical servo structure composed of PI velocity loop and P position loop, provided that its transfer function has real zeros. This in turn requires the ratio T_I/T_D of the integral time $T_I = k_P/k_I$ to the derivative time $T_D = k_D/k_P$ to be no smaller than 4. If $T_I/T_D = 4$, as in the familiar Ziegler-Nichols tuning rules [13], the PID transfer function can be written as

$$G_{\mathrm{PID}}(s) = k_R \frac{(s+\alpha)^2}{s} \tag{2a}$$

with

$$k_R = k_P \frac{T_I}{4} \quad \text{and} \quad \alpha = \frac{2}{T_I}. \tag{2b}$$

So it is a PID controller with a double real zero $-\alpha$ and equivalent gain k_R. Taking into account the double integrator, the open-loop transfer function

$$G_{\mathrm{open}}(s) = K \frac{(s+\alpha)^2}{s^3}, \qquad K = k_R k_o \tag{3}$$

is of 3rd order. Conversion of the P-PI structure into PID generates the filter (see Section 4)

$$F(s) = \frac{\alpha}{s+\alpha}. \tag{4}$$

Root-locus plot of the closed-loop poles shown in Fig. 2a consists of two circular branches meeting at the double pole s_2 and the 3rd real branch approaching the zero $-\alpha$. To get smooth, critically damped responses we have to choose the open-loop gain K corresponding to s_2. From the root-locus breakpoint condition $dG_{\mathrm{open}}/ds = 0$ one obtains

$$s_2 = -3\alpha, \quad K = \frac{27}{4}\alpha, \quad s_1 = -\frac{3}{4}\alpha. \tag{5}$$

The pole s_1 follows from the division of the closed-loop characteristic polynomial $s^3 + K(s+\alpha)^2$ by $(s-s_2)^2$.

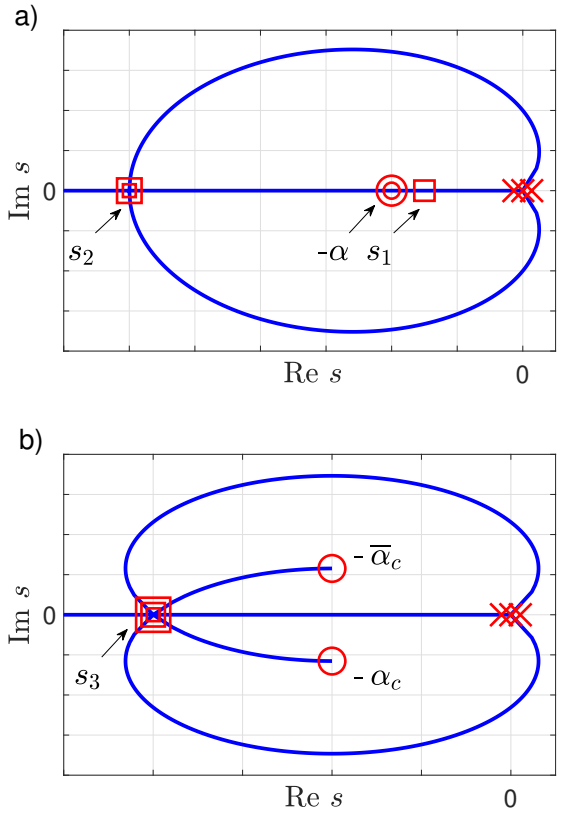

Fig. 2. Root-locus plot for the PID control system with: a) double real zero, b) complex zeros (× – open-loop pole, ○ – open-loop zero, □ – closed-loop pole)

Let the system dynamic be specified by a required settling time t_s. Since t_s is determined by the dominant pole s_1 close to $-\alpha$ (which speeds up the transient), so taking $t_s \cong 3/|s_1|$ gives the modulus of the controller zero as

$$\alpha = \frac{4}{t_s}. \tag{6}$$

Using it in (5) and (2b) yields the following PID settings

$$k_P = \frac{216}{t_s^2 k_o}, \quad k_I = \frac{432}{t_s^3 k_o}, \quad k_D = \frac{27}{t_s k_o}. \tag{7}$$

2.2. Pole placement

To get a triple closed-loop time constant λ as in IMC (Appendix) we remove the condition $T_I/T_D \geq 4$ required by the transformation of PID to P-PI. The following pole placement equation for the denominator of the closed-loop transfer function holds

$$s^3 + k_o\left(k_D s^2 + k_P s + k_I\right) = (s+p)^3, \quad p = 1/\lambda\,. \tag{8}$$

Equating coefficients of the polynomials on both sides gives

$$k_P = \frac{3}{\lambda^2 k_o}, \quad k_I = \frac{1}{\lambda^3 k_o}, \quad k_D = \frac{3}{\lambda k_o} \tag{9}$$

(compare Appendix). Here the ratio $T_I/T_D = {k_P}^2/(k_I k_D)$ equals 3, which implies complex zeros of the new controller. So its transfer function can be written as

$$G_{\mathrm{PID}}(s) = K\frac{(s+\alpha_c)(s+\overline{\alpha}_c)}{s}, \quad K = \frac{3}{\lambda k_o}, \tag{10a}$$

with the complex zero

$$-\alpha_c = -\frac{1}{2\lambda}\left(1 + j\frac{1}{\sqrt{3}}\right). \tag{10b}$$

To illustrate the difference from the previous design, root-locus plot of the new system for varying K is shown in Fig. 2b. By construction, the triple pole s_3 of the closed-loop system equals $-1/\lambda$ and is reached for K in (10a). Unlike the previous plot (Fig. 2a), where the double zero $-\alpha$ stops the real branch at s_1, here the complex zeros open up the way for this branch to meet the two circular branches at s_3.

2.3. Tunings

Assume as before that a required settling time t_s and the servo gain k_o are given. For the triple time constant λ we may write $t_s \cong 8\lambda$, so $\lambda \cong t_s/8$. Now according to (9)

$$k_P = \frac{192}{t_s^2 k_o}, \quad k_I = \frac{512}{t_s^3 k_o}, \quad k_D = \frac{24}{t_s k_o}. \tag{11}$$

So the new settings are only slightly different from the previous ones in (7), hence very similar behavior may be expected. It is also natural to assume the reference filter as

$$F(s) = \frac{\mathrm{Re}\,\alpha_c}{s + \mathrm{Re}\,\alpha_c}, \tag{12}$$

where $\mathrm{Re}\,\alpha_c = 1/(2\lambda) = 4/t_s$, i.e. the same as α in (6).

If natural frequency ω_n is the preferred specification parameter to calculate the settings, the corresponding settling time follows from $t_s \cong 4/\omega_n$ [5] (for unity damping ratio).

The experimental step response of the designed PID system strictly corresponding to P-PI is shown in Section 6, as well as the response when the derivative action involves additional filtering.

2.4. Frequency characteristics

To compare the robustness of the pole placement and root-locus designs one can check sensitivity with respect to the servo gain k_o which may be inaccurately determined. Sensitivities $|dG_{\mathrm{closed}}/dk_o|$ of the closed-loop transfer function for $k_o = 1$, $\lambda = 1$ ($t_s = 8$) in relevant frequency range are shown in Fig. 3. As seen, the pole placement design is slightly more sensitive to k_o than the root-locus.

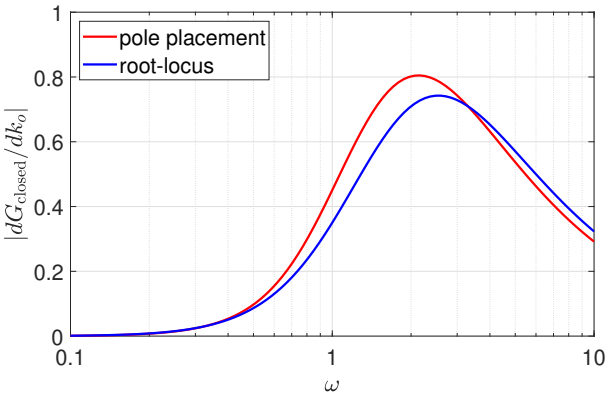

Fig. 3. Sensitivities of closed-loop transfer functions with respect to k_o

3. DISCRETE PID CONTROLLER

3.1. Basic derivation

If a PLC implementing a continuous control algorithm cannot sample fast enough, in particular two hundred times per settling time for P-PI [10], the continuous design should be transformed into equivalent discrete form. So let Δ denote a discretization step (control cycle). Discrete time transfer function of the double integrator k_o/s^2 has the following form [1, 5]

$$G_o(z) = k_o\frac{\Delta^2}{2}\frac{z+1}{(z-1)^2}. \tag{13a}$$

Likewise the PID controller becomes

$$G_{\mathrm{PID}}(z) = k_P + k_I\Delta\frac{z}{z-1} + \frac{k_D}{\Delta}\frac{z-1}{z} = \frac{k_1 z^2 - k_2 z + k_3}{z(z-1)}, \tag{13b}$$

where

$$k_1 = k_P + k_I\Delta + \frac{k_D}{\Delta}, \quad k_2 = k_P + 2\frac{k_D}{\Delta}, \quad k_3 = \frac{k_D}{\Delta}. \tag{13c}$$

The open-loop transfer function takes the form

$$G_{\mathrm{open}}(z) = \frac{(z+1)(K_1 z^2 - K_2 z + K_3)}{z(z-1)^3} \tag{14a}$$

with

$$K_i = k_o k_i \frac{\Delta^2}{2} \tag{14b}$$

for $i = 1,2,3$. Therefore the denominator of the closed-loop transfer function becomes

$$f(z) = z(z-1)^3 + (z+1)(K_1 z^2 - K_2 z + K_3). \tag{15}$$

Following the continuous case, we want $f(z)$ to have a triple root

$$r = e^{-p\Delta} \tag{16}$$

with $p = 1/\lambda$.

It is known that if a function $f(z)$ has a root r of multiplicity k, then

$$f(r) = f'(r) = f''(r) = \ldots = f^{(k-1)}(r) = 0. \tag{17}$$

Applying these conditions to $f(z)$ for $k = 3$ one obtains a system of three equations linear with respect to K_1, K_2 and K_3, having the solution [14]

$$\begin{aligned} K_1 &= C(3r^3 + 8r^2 + 5r - 4), \\ K_2 &= C(3r^4 + 12r^3 + 14r^2 - 4r - 1), \\ K_3 &= Cr^3(r^2 + 4r + 7), \end{aligned} \tag{18a}$$

where

$$C = \frac{1-r}{(r+1)^3}. \tag{18b}$$

3.2. Interval for *r*

For a feasible value of r (see below), root-locus plot with respect to the open-loop gain is shown in Fig. 4. The right part of the plot with the triple breakpoint $z_3 = r$ corresponds to continuous case (Fig. 2b), whereas the left one with the pole z_1 reflects the increased order of $G_{\text{open}}(z)$ from (14a) compared to its continuous counterpart. The analytic expression for z_1 may be obtained from the division

$$\frac{f(z)\big|_{K_1(r),K_2(r),K_3(r)}}{(z-r)^3} = z - z_1, \tag{19}$$

which gives

$$z_1 = \frac{(1-r)(r^2+4r+7)}{(r+1)^3} = \frac{K_3}{r^3}. \tag{20}$$

With decreasing r the right and left part of the plot (Fig. 4) converge and meet at some value of r for which the equation $z_1(r) = r$ holds. The only real solution of this equation gives $r = r_4 = \sqrt[4]{8} - 1 \cong 0.682$, i.e. the unique quadruple real pole of the closed-loop transfer function. Analytic properties of the expression (20) assert that if $r \in [r_4, 1)$ then $z_1 \in (0, r_4]$, hence the system is stable and its dynamic is dominated by the triple pole r or the quadruple if $r = r_4$.

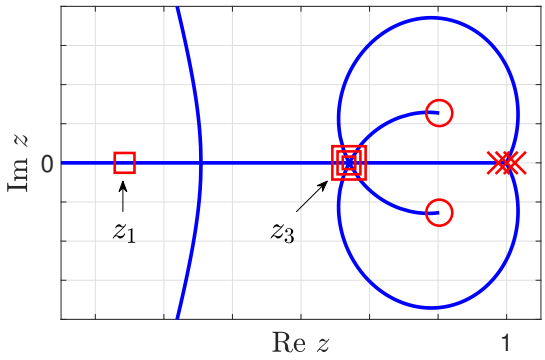

Fig. 4. Root-locus for discrete PID

3.3. Discretization step

The discrete form of the controller requires evaluation of the step Δ for which the design is feasible. The admissible Δ is determined by the lower limit condition $r \geq r_4$. Using (16) for $r_4 = 0.682$ yields $\Delta \leq -(\ln r_4)/p$ or $\Delta \leq 0.383\lambda$. Since $\lambda \cong t_s/10$ for the quadruple time constant limit, we get

$$\Delta \leq \frac{t_s}{26}, \tag{21}$$

which is the requirement for discrete implementation providing the settling time t_s.

Analogous requirement for the discrete P-PI (or, equivalently, PID with a reference filter) having a double real zero yields $\Delta \leq t_s/45$ [10]. Thus the benefit from the pole placement design rests in almost twice longer limit on the discretization step than in the former case.

3.4. Tunings and responses

Given a required settling time t_s, gain k_o, and step Δ one should determine the corresponding value of r from (16) with $p = 1/\lambda$, $\lambda = t_s/8$, i.e. $r = \exp(-8\Delta/t_s)$. If the condition $r \geq r_4 (= 0.682)$ does not hold, larger t_s must be chosen. Then the parameters K_1, K_2, K_3 need to be calculated according to (18) and, finally, the target settings obtained by the formulas

$$k_P = \frac{2(K_2 - 2K_3)}{k_o \Delta^2}, \quad k_I = \frac{2(K_1 - K_2 + K_3)}{k_o \Delta^3}, \quad k_D = \frac{2K_3}{k_o \Delta} \tag{22}$$

derived from (13c) and (14b). Analytic properties of the functions (18) assert that $K_2 - 2K_3 > 0$, $K_1 - K_2 + K_3 > 0$ and $K_3 > 0$ for $r \in [r_4, 1)$. Hence (22) provide realizable settings of the discrete PID controller.

In practical applications it could be often more convenient to calculate the settings from

$$k_P = \frac{\rho_P}{950 k_o \Delta^2}, \quad k_I = \frac{\rho_I}{9400 k_o \Delta^3}, \quad k_D = \frac{\rho_D}{230 k_o \Delta}, \tag{23}$$

after reading out the values ρ_P, ρ_I, and ρ_D from the nomograms in Fig. 5 for a given r. The nomograms have been obtained by combining (18) and (22).

Simulated step responses for the discrete PID and the P-PI from [10] are compared in Fig. 6. The controller settings are

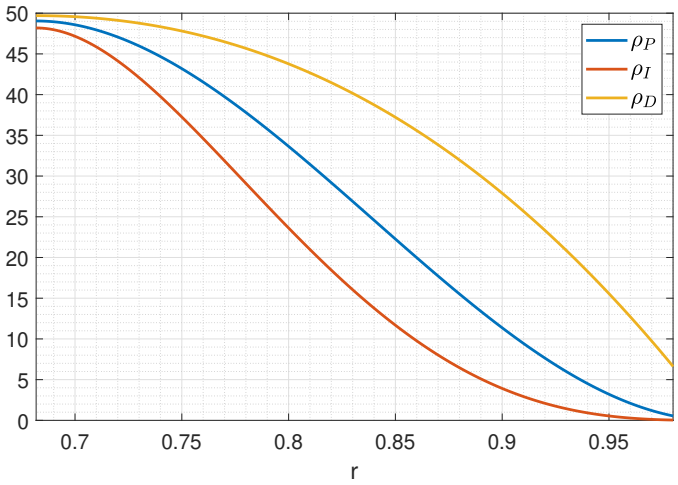

Fig. 5. Nomograms for the discrete PID controller settings

calculated for the discretization step $\Delta = 0.015$ s as in laboratory experiments in Section 6. It implies the approximate lower bounds on settling time equal to $26\Delta \cong 0.4$ s and $45\Delta \cong 0.7$ s for the PID and P-PI, respectively. One can try to ignore the condition $\Delta \leq t_s/45$ for P-PI to obtain a system as fast as for PID, but then the step response becomes oscillatory (Fig. 6).

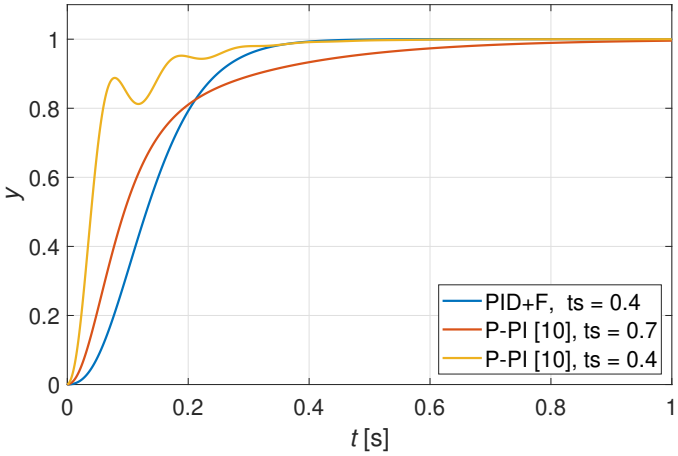

Fig. 6. Step responses for the considered discrete PID and the P-PI proposed in [10]

4. CONTINUOUS PI-PI CONTROL

4.1. Control structures

By applying PI control both for velocity and position loops we get the system of Fig. 7a, where

$$PI_V(s) = k_{PV} + \frac{k_{IV}}{s}, \qquad PI_P(s) = k_P + \frac{k_I}{s}. \tag{24}$$

Additional integral in the position loop improves the accuracy of servos tracking complicated trajectories and suppressing varying disturbances. The two loops may be replaced by a

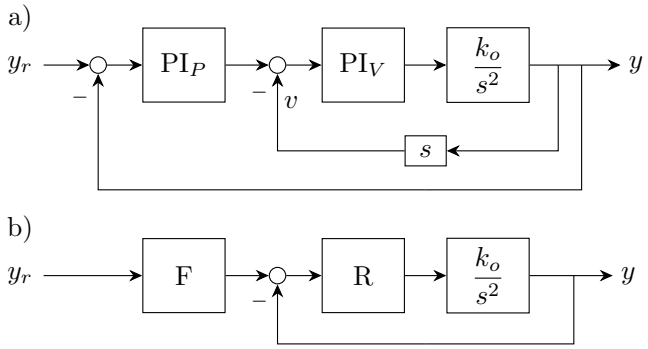

Fig. 7. a) PI-PI servo control system, b) single-loop equivalent

single one of Fig. 7b, where [10]

$$R(s) = \frac{(k_{PV}s + k_{IV})(s^2 + k_P s + k_I)}{s^2}, \tag{25a}$$

$$F(s) = \frac{k_P s + k_I}{s^2 + k_P s + k_I}. \tag{25b}$$

Before going into design issues note that by setting k_I to 0 we get the classical P-PI structure represented by

$$R(s)\big|_{k_I=0} = \frac{(k_{PV}s + k_{IV})(s + k_P)}{s}, \qquad F(s)\big|_{k_I=0} = \frac{k_P}{s + k_P}. \tag{26}$$

So $R(s)$ for $k_I = 0$ is just the PID controller of Fig. 1. As seen from above, such a controller may have real zeros only. If $k_P = k_{IV}/k_{PV}$, it has a double zero equal to $-\alpha$ in (2a).

4.2. Pole placement

For notational convenience, let us rewrite (25a) as

$$R(s) = K\frac{(s+\alpha)(s^2 + \beta s + \gamma)}{s^2} \tag{27a}$$

with

$$K = k_{PV}, \quad \alpha = \frac{k_{IV}}{k_{PV}}, \quad \beta = k_P, \quad \gamma = k_I. \tag{27b}$$

The open-loop transfer function $G_{\text{open}}(s) = R(s)k_o/s^2$ is now of 4th order, so a quadruple pole may be required.

To simplify development we introduce normalization with respect to α, obtaining the open-loop transfer function

$$G_{\text{open}}(s) = K'\frac{(s'+1)(s'^2 + \beta' s' + \gamma')}{s'^4}, \tag{28a}$$

with

$$s' = \frac{s}{\alpha}, \quad K' = \frac{Kk_o}{\alpha}, \quad \beta' = \frac{\beta}{\alpha}, \quad \gamma' = \frac{\gamma}{\alpha^2}. \tag{28b}$$

Characteristic polynomial of the closed-loop transfer function becomes

$$f(s') = s'^4 + K'(s'+1)(s'^2 + \beta' s' + \gamma'). \tag{29}$$

We want this polynomial to have a quadruple root s'_4, so

$$f(s') = \left(s' - s'_4\right)^4. \tag{30}$$

Equating coefficients of the expanded forms of (29) and (30) yields the simple solution

$$K' = 8, \quad \beta' = 2, \quad \gamma' = 2, \quad s'_4 = -2. \tag{31}$$

One may comment that the solution can also be obtained from the equations $f(s'_4) = f'(s'_4) = f''(s'_4) = f'''(s'_4) = 0$ (see (17) in Section 3). Roots of the polynomial $s'^2 + 2s' + 2$, i.e. normalized zeros of the controller, are $-1 \pm j1$.

4.3. Tunings

As before, assume that a settling time t_s and gain k_o are given. For the quadruple pole $s_4 = s'_4\alpha = -2\alpha$ one may write $t_s \cong 10/|s_4|$, hence

$$\alpha \cong \frac{5}{t_s}. \tag{32}$$

Values of the remaining parameters K, β, γ follow from (28b) and those of the PI controllers from (27b). Finally, one obtains the settings for the pair of controllers

$$\begin{aligned} k_P &= \frac{10}{t_s}, \qquad k_I = \frac{50}{t_s{}^2}, \\ k_{PV} &= \frac{40}{t_s k_o}, \quad k_{IV} = \frac{200}{t_s{}^2 k_o}. \end{aligned} \tag{33}$$

Step and ramp responses for such settings are presented in Section 6.

4.4. Idea of the previous design [10]

Although not necessary, the term $s^2 + k_P s + k_I$ in (25a) has been assumed to have a double root $-\beta$, analogously as in the P-PI case. So the controller transfer function becomes

$$R(s) = K\frac{(s+\alpha)(s+\beta)^2}{s^2}. \tag{34}$$

The corresponding root-locus plot shown in Fig. 8a has two breakpoints s_{b1} and s_{b2}. Critically damped responses are obtained when the two breakpoints are reached simultaneously. This condition yields the following solution

$$K = \frac{16\alpha}{k_o}, \quad \beta = 2\alpha. \tag{35}$$

Settling time is determined by the pair of dominant poles in the breakpoint

$$s_{b1} = -2(2-\sqrt{2})\alpha \cong -1.17\alpha.$$

In the pole placement case, instead of the two breakpoints, we have one quadruple breakpoint s'_4 as in Fig. 8b, where the internal and external branches meet.

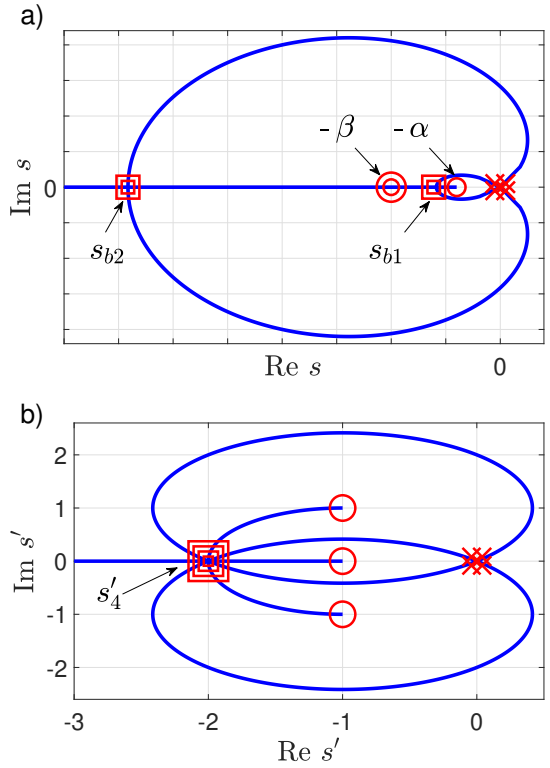

Fig. 8. Root-locus plot for PI-PI structure with: a) three real zeros (β double), b) two complex zeros and a real one

5. DISCRETE PI-PI CONTROL

We follow the steps of Section 3 with some extensions.

5.1. Basic derivation

Discrete implementation of the PI-PI system from Fig. 7a consists of the double integrator (13a) and the controllers

$$\begin{aligned} G_{PIp}(z) &= k_P + k_I\Delta\frac{z}{z-1}, \\ G_{PIv}(z) &= k_{PV} + k_{IV}\Delta\frac{z}{z-1}, \end{aligned} \tag{36}$$

whith the operator s replaced by $(z-1)/(\Delta z)$. As before, the two loops are equivalent to the single one of Fig. 7b with [10]

$$R(z) = k_R\frac{(z-\alpha)(z-\beta)(z-\gamma)}{\Delta z(z-1)^2}, \tag{37a}$$

$$F(z) = \frac{\Delta z\left[(k_P + k_I\Delta)z - k_P\right]}{(k_I\Delta^2 + k_P\Delta + 1)(z-\alpha)(z-\beta)}, \tag{37b}$$

where

$$\begin{aligned} k_R &= (k_{PV} + k_{IV}\Delta)(k_I\Delta^2 + k_P\Delta + 1), \\ \alpha\beta &= \frac{1}{k_I\Delta^2 + k_P\Delta + 1}, \\ \alpha + \beta &= \frac{k_P\Delta + 2}{k_I\Delta^2 + k_P\Delta + 1}, \\ \gamma &= \frac{k_{PV}}{k_{PV} + k_{IV}\Delta}. \end{aligned} \tag{38}$$

In [10] it was assumed that α, β, γ are real ($\mathbb{R}$). However, since the formulas above express the product and sum of the zeros α, β, they remain correct also for complex ($\mathbb{C}$) case provided that

$$\beta = \overline{\alpha} \in \mathbb{C}, \qquad \gamma \in \mathbb{R}. \tag{39}$$

We want the closed-loop system with a quadruple pole $z_4 = r$.

Let us rewrite $R(z)$ in the form similar to PID in (13b), i.e. with the numerator linear with respect to the coefficients

$$R(z) = \frac{k_1 z^3 - k_2 z^2 + k_3 z - k_4}{z(z-1)^2}. \tag{40}$$

For such $R(z)$ the denominator of the closed-loop transfer function becomes

$$f(z) = z(z-1)^4 + (z+1)(K_1 z^3 - K_2 z^2 + K_3 z - K_4) \tag{41}$$

with K_i, $i = 1,\ldots,4$ defined in (14b). Applying the condition (17) with the multiplicity $k = 4$ to $f(z)$ above, we get a system of four equations linear with respect to $K_1,\ldots,K_4$. Its solution has the form [14]

$$\begin{aligned} K_1 &= C(4r^4 + 15r^3 + 19r^2 + 5r - 11), \\ K_2 &= C(6r^5 + 30r^4 + 55r^3 + 35r^2 - 25r - 5), \\ K_3 &= C(4r^6 + 20r^5 + 44r^4 + 45r^3 - 11r^2 - 5r - 1), \\ K_4 &= Cr^4(r+3)(r^2 + 2r + 5), \end{aligned} \tag{42a}$$

where

$$C = \frac{1-r}{(r+1)^4}. \tag{42b}$$

Comparing (37a) with (40) and taking into account (14b), we get

$$k_R = \frac{2K_1}{k_o \Delta} \tag{43}$$

and α, β, γ as the roots of the equation $K_1 z^3 - K_2 z^2 + K_3 z - K_4 = 0$. Assuming $K_1 \neq 0$, it is a cubic equation in a general form whose real root γ, as well as the product $a = \alpha\beta$ and the sum $b = \alpha + \beta$ of the two other roots can be consecutively obtained from the following expressions to satisfy the conditions (39)

$$\begin{aligned} \delta &= \frac{27{K_1}^2 K_4 - 9K_1 K_2 K_3 + 2{K_2}^3}{54{K_1}^3} \\ &\quad + \frac{\sqrt{27{K_1}^2{K_4}^2 + (4{K_2}^3 - 18K_1K_2K_3)K_4 + 4K_1{K_3}^3 - {K_2}^2{K_3}^2}}{3^{3/2}2{K_1}^2}, \\ \gamma &= \sqrt[3]{\delta} - \frac{3K_1K_3 - {K_2}^2}{9\sqrt[3]{\delta}{K_1}^2} + \frac{K_2}{3K_1} \in \mathbb{R}, \\ a &= \alpha\beta = \frac{K_4}{\gamma K_1} \in \mathbb{R}, \quad b = \alpha + \beta = \frac{K_2 - \gamma K_1}{K_1} \in \mathbb{R}, \end{aligned} \tag{44}$$

where δ is an auxiliary variable calculated first to get γ.

5.2. Intervals for r and Δ

The general shape of root-locus plot (not shown) is very similar to the one of Fig. 4, but with the right part replaced by discrete version of Fig. 8b. The fifth single pole z_1 is obtained by substituting (42) into (41) and dividing the resulting $f(z)$ by $(z-r)^4$. This yields

$$z_1 = \frac{(1-r)(r+3)(r^2+2r+5)}{(r+1)^4} = \frac{K_4}{r^4}. \tag{45}$$

As before, the equation $z_1(r) = r$ gives the unique real solution $r_5 = \sqrt[5]{16} - 1 \cong 0.741$ that represents the quintuple pole of the closed-loop system. Moreover, properties of the expression (45) imply that if $r \in [r_5, 1)$ then $z_1 \in (0, r_5]$, hence the system is stable with the dominant pole r.

This time the condition $r \geq r_5$ yields $\Delta \leq 0.3\lambda$, so for $t_s \cong 12\lambda$ (quintuple λ) we get

$$\Delta \leq \frac{t_s}{40}. \tag{46}$$

This is considerably better than $t_s/130$ in [10] where the double real zero prevented getting the quadruple pole (see Fig. 8a).

5.3. Tunings and responses

Having k_R, a, b, γ calculated from (43) and (44), the original parameters of the controllers are obtained by solving (38). Hence

$$\begin{aligned} k_P &= \frac{b - 2a}{a\Delta}, \qquad k_I = \frac{1 + a - b}{a\Delta^2}, \\ k_{PV} &= a\gamma k_r, \qquad k_{IV} = \frac{a(1-\gamma)k_r}{\Delta}. \end{aligned} \tag{47}$$

As in Section 3 we can combine the formulas (42), (43), (44), (47) to get the following compact expressions for the settings

$$\begin{aligned} k_P &= \frac{\rho_P}{300\Delta}, \qquad k_I = \frac{\rho_I}{2000\Delta^2}, \\ k_{PV} &= \frac{\rho_{PV}}{110 k_o \Delta}, \qquad k_{IV} = \frac{\rho_{IV}}{930 k_o \Delta^2}. \end{aligned} \tag{48}$$

The coefficients ρ_P, ρ_I, ρ_{PV}, ρ_{IV} are read out from the nomograms in Fig. 9 for a given r. The nomograms confirm that the PI-PI structure is realizable for the quadruple pole placement, since all the settings are positive for $r \in [r_5, 1)$.

Simulated step responses for the PI-PI controllers with the settings developed in this section and those proposed in [10] are compared in Fig. 10. The discretization step $\Delta = 0.015$ s is used as in Section 3. Approximate lower bounds on settling time are $40\Delta \cong 0.6$ s and $130\Delta \cong 2.0$ s for the new PI-PI settings and the previous ones from [10], respectively. Again, one can try to ignore the condition $\Delta \leq t_s/130$ attached to the formulas from [10] to have the settling time 0.6 s, but this leads to an unstable system. The stability limit is reached for the settling time 0.75 s, as shown in Fig. 10.

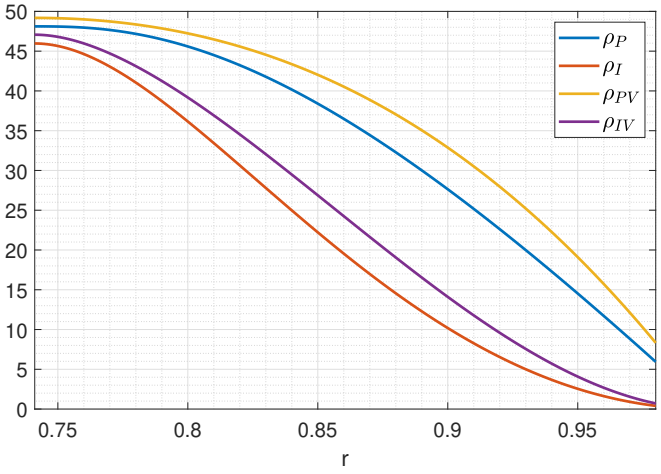

Fig. 9. Nomograms for the discrete PI-PI control structure settings

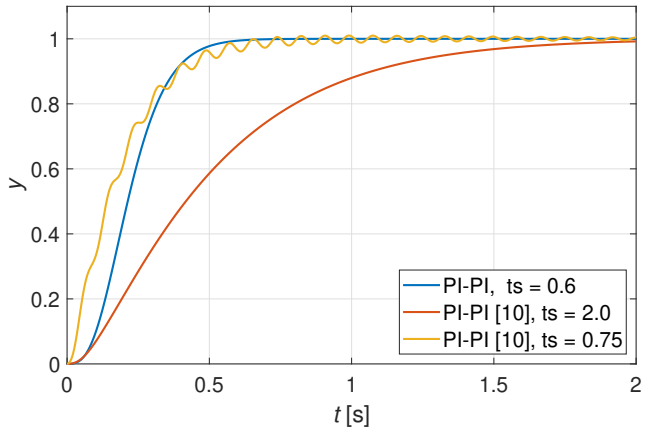

Fig. 10. Step responses for the considered discrete PI-PI and the PI-PI proposed in [10]

6. EXPERIMENTAL RESULTS

A laboratory servo system shown in Fig. 11 has been set-up to verify the designs. It consists of a ball screw linear actuator, Estun AC servomotor and servo drive [15] with EtherCAT bus, Beckhoff C6920 industrial PC [16] for PLC code execution, and standard PC with TwinCAT 3 engineering software for programming. The continuous and discrete controllers have been implemented in ST (Structured Text) language as function blocks of the IEC 61131-3 standard [17]. All calculations described by the formulas (11), (18), (22) for PID, and (33), (42), (43), (44), (47) for PI-PI have been embedded in a PLC program to compute target settings for given data. Although some of the formulas look complicated, they can be expressed by elementary ST instructions, including EXPT function for the cube root in (44).

The servo has been controlled using a combined reference trajectory composed of step and ramp parts shown in Fig. 12. Disturbance has been simulated by a signal added to controller output.

The discrete control algorithms have been running with the cycle $\Delta = 15$ ms. Their settings have been calculated for the multiple poles corresponding to the shortest settling time, i.e. for the design parameter $r = r_4 = 0.682$ in the case of PID (Section 3) and $r = r_5 = 0.741$ in the case of PI-PI (Section 5). Continuous algorithms have been emulated by the Euler backward approximation executed with the shortest cycle $\Delta_{\min} = 1$ ms available in the lab system.

Step responses of the originally designed discrete controllers exhibit overshoots due to zeros of the transfer functions. Hence the reference filters have to be added. Zeros of the PID controller are the roots (complex) of the polynomial $K_1 z^2 - K_2 z + K_3$. Following the continuous filter (12), one can apply its 1st order discrete counterpart

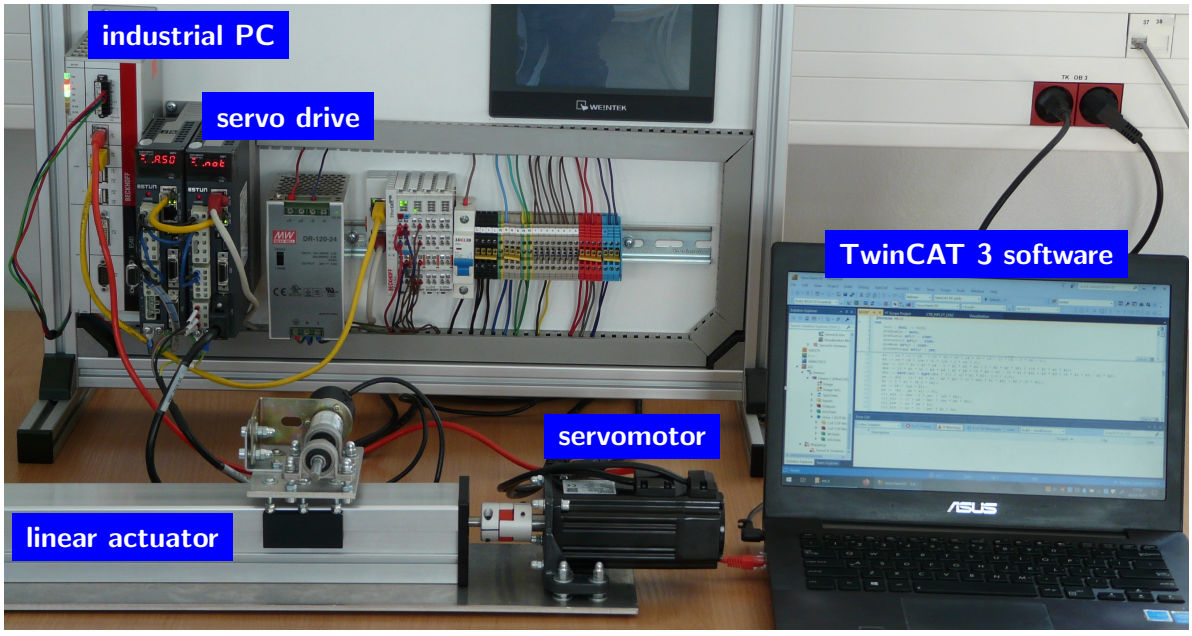

Fig. 11. Laboratory servo system

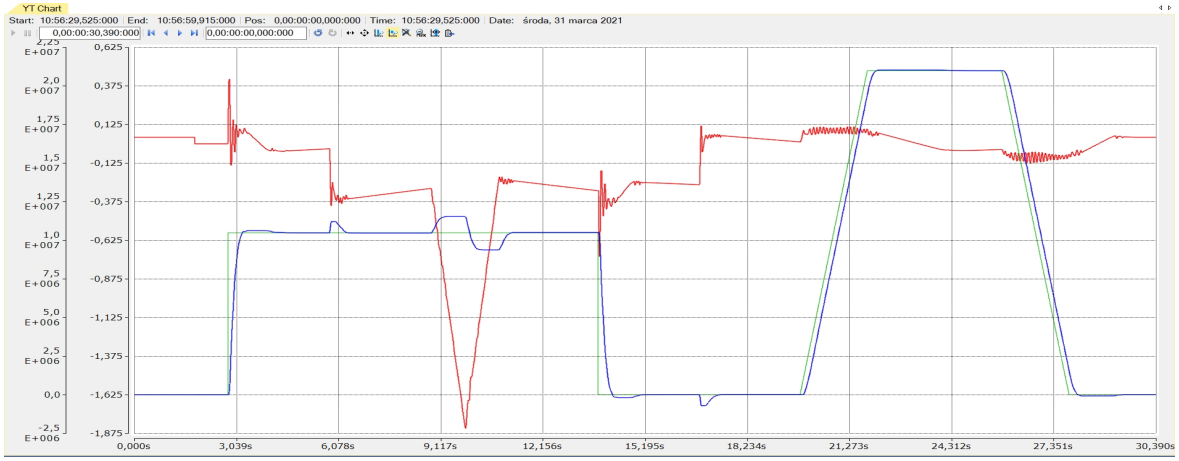

Fig. 12. Experimental results recorded by TwinCAT 3 software: green – reference position, blue – actual position, red – control output

$$F_{1,\mathrm{PID}}(z) = \frac{(1-z_f)z}{z-z_f}, \tag{49}$$

where z_f denotes the real part of the zeros, i.e. $z_f = 0.5K_2/K_1$. The full 2nd order filter

$$F_{2,\mathrm{PID}}(z) = \frac{(K_1-K_2+K_3)z^2}{K_1z^2-K_2z+K_3}, \tag{50}$$

slightly more complicated, cancels out both zeros.

The discrete PI-PI control structure has two real zeros

$$z_{fa} = \frac{k_P}{k_P+k_I\Delta}, \qquad z_{fb} = \frac{k_{PV}}{k_{PV}+k_{IV}\Delta}, \tag{51}$$

where z_{fa} emerges in the connection of $R(z)$ from (37a) with $F(z)$ from (37b) according to the diagram in Fig. 7b, and z_{fb} follows from (37a) and (38). One can eliminate the zero z_{fa} by the reference filter

$$F_{1,\mathrm{PI\text{-}PI}}(z) = \frac{(1-z_{fa})z}{z-z_{fa}} \tag{52}$$

or, equivalently, by splitting the position PI controller to get the I-P-PI structure proposed in [10]. If the filter (52) turns out insufficient, one can use the following variant

$$F_{2,\mathrm{PI\text{-}PI}}(z) = \frac{(1-z_{fa})(1-z_{fb})z^2}{(z-z_{fa})(z-z_{fb})} \tag{53}$$

that cancels both zeros.

Comparison of experimental step responses for the two controllers (PID, PI-PI) and related filters (F1, F2) is presented in Fig. 13a. The configuration PID+F1 works correctly in general, however, the motion is not smooth, with oscillations of velocity. There is no such behavior in the case of PID+F2. The structure PI-PI+F2 settles down aperiodically, whereas PI-PI+F1 exhibits an overshoot of about 10%. Barely visible oscillations in the vicinity of y_r are due to static friction. Experimental responses for the P-PI and PI-PI controllers tuned according to [10] are also presented in Fig. 13a. Their settling times are longer, particularly for the PI-PI, as shown earlier in Sections 3 and 5.

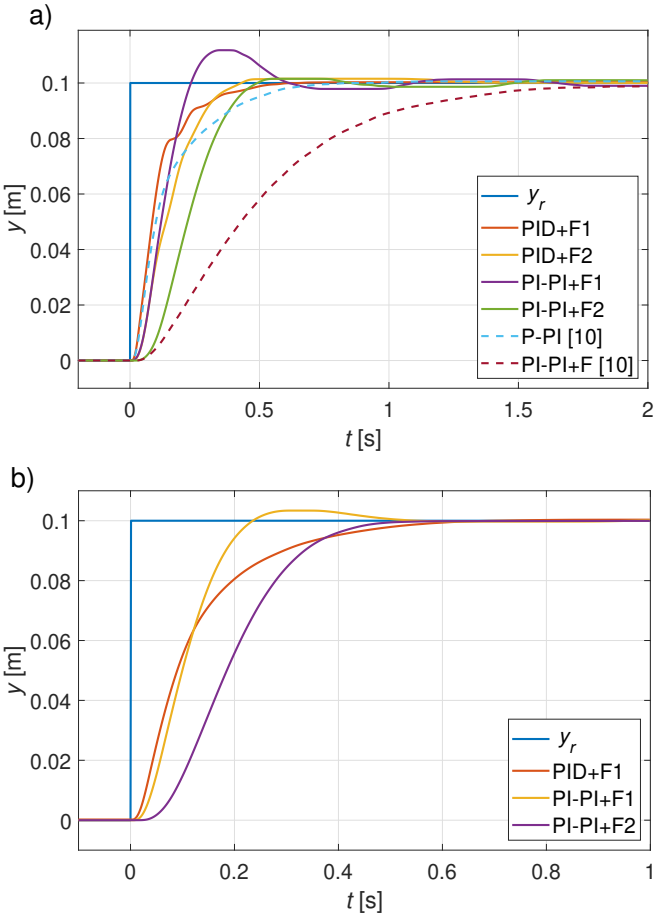

Fig. 13. Step responses of control structures: a) discrete, b) continuous

The filters F2 in the structures PID+F2 and PI-PI+F2 cancel all zeros affecting the shape of responses. Therefore the settling times determined by (21) and (46) may be expected, namely $t_s^{\mathrm{PID}} \geq 26 \cdot 0.015$ s $\cong 0.4$ s and $t_s^{\mathrm{PI\text{-}PI}} \geq 40 \cdot 0.015$ s $= 0.6$ s, for PID+F2 and PI-PI+F2, respectively. As seen from Fig. 13a the actual settling times are close to the estimates. Table 1 collects them and compares them with those obtained for the double zero design [10]. The approximate minimum settling times

Table 1
Settling times of discrete control structures

Controller	Multiple pole		Double zero [10]	
	MIN	EX	MIN	EX
PID / P-PI	26Δ	0.4 s	45Δ	0.7 s
PI-PI	40Δ	0.6 s	130Δ	2.0 s

(MIN) in terms of Δ are given, along with the values obtained in the experiments for $\Delta = 15$ ms (EX).

The continuous control has been emulated for the shortest available cycle $\Delta_{\min} = 1$ ms. The controllers are tuned for $t_s = 0.5$ s, being actually the average of settling times obtained in the discrete control (0.4 vs. 0.6 s). Experimental step responses are presented in Fig. 13b. The responses of the structures without reference filters exhibit overshoots, as in the case of discrete controllers. The control structure PID+F1 with the filter (12) completely eliminates the overshoot. For the PI-PI structure, the inertial filter

$$F_{1,\text{PI-PI}}(s) = \frac{k_I}{k_P s + k_I} = \frac{1}{\frac{t_s}{5}s + 1} \tag{54}$$

is applied, which is equivalent to splitting the position PI into I and P, as proposed in [10]. However, this filter leaves a few percent overshoot. To eliminate the overshoot completely, the following extended filter can be used

$$F_{2,\text{PI-PI}}(s) = \frac{k_I}{k_P s + k_I} \cdot \frac{k_{IV}}{k_{PV} s + k_{IV}} = \frac{1}{\left(\frac{t_s}{5}s + 1\right)^2}. \tag{55}$$

All the responses are smooth and settle down according to the assumed settling time 0.5 s.

Note that for $\Delta_{\min} = 1$ ms we may get the shortest settling time $t_s = 26$ ms $\cong 30$ ms of the discrete PID servo control provided by the Beckhoff PLC or other modern PLCs.

The integral actions of the plant and controllers should provide exact tracking of higher-order reference trajectories. Of course, the tracking will be error-free only without the reference filters which, as shown for the ramps in Figs. 14a, b, introduce unavoidable delays.

Control error responses of continuous structures due to disturbances acting at steady-state are compared in Fig. 15. Although the PI-PI structure suppresses the step and ramp disturbance much better, it suffers from a visible limit cycle due to friction. So in practice a tracking PI-PI controller may switch into PID control mode while approaching the steady-state. Guidelines on how to reduce to some extent the effect of friction on servo behavior can be found in [2, 3].

In practical implementations, so-called real PID algorithm is most often used with the filtered derivative block, here in the form $k_D s/(T_D s/D + 1)$, $T_D = k_D/k_P$, to suppress measurement noise and high-frequency disturbances. In the experiments, two implementations of the continuous PID with the reference filter (12) have been compared: 1) basic derivative $k_D s$ (PID),

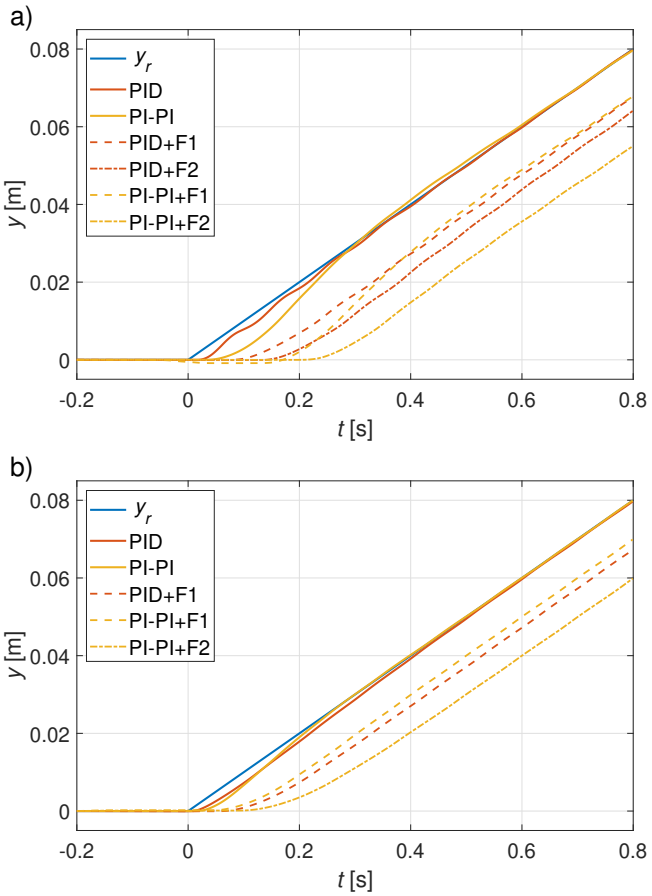

Fig. 14. Ramp tracking for control structures: a) discrete, b) continuous

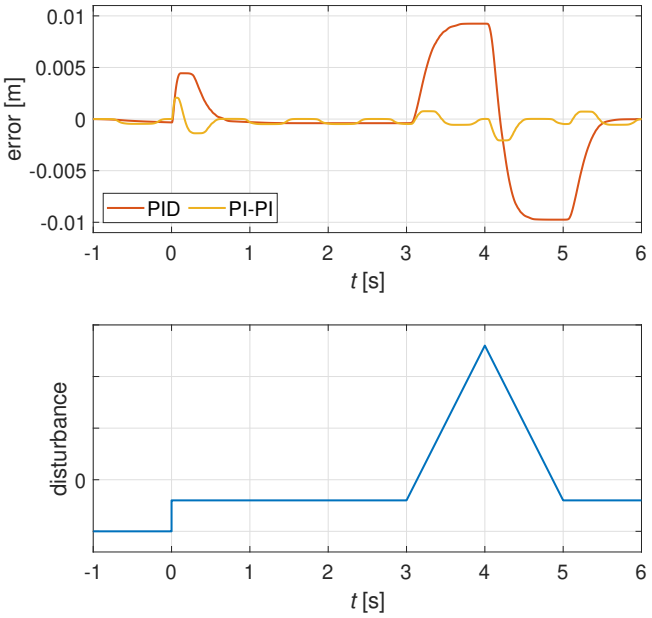

Fig. 15. Disturbance suppression in continuous control structures

2) real version as above with $D = 5$ (PIDR). Note that $D = 5$ is a default value in a number of industrial controllers. As seen in Fig. 16, step responses of the position y almost overlap. How-

ever, the control signal u for the PIDR is a decaying oscillation due to the increased order of the system and unchanged settings. Since high-resolution encoder is used in the servo, the oscillations may be easily reduced by increasing D. Nevertheless, extension of the pole placement method on arbitrary D in the real PID remains a subject of future work.

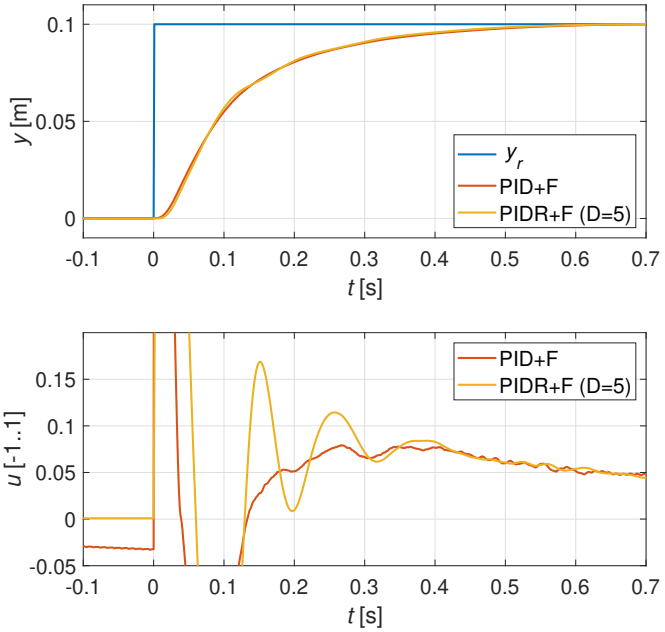

Fig. 16. Step responses of the servos with ideal and real continuous PID controllers

7. CONCLUSIONS

New tuning rules for PID and PI-PI servo controllers have been derived using multiple pole placement approach, as an alternative to the root-locus design [10]. The root-locus assumes real zeros of the PID controller, so it can be converted into the classical P-PI two-loop structure. This is not the case for the pole placement PID which has complex zeros, so it must be implemented in a standard single loop. The new approach admits twice longer control cycle for the discrete PID and four times for PI-PI. This in turn implies that twice or four times shorter settling times can be obtained for the same control cycle. Shorter settling time may be important in the case of high-performance servos, whereas longer control cycle suits heavily loaded PLCs executing demanding tasks in parallel. Actually, the pole placement approach has been motivated by an earlier IMC solution for a double integrator.

Nomograms for tuning the discrete PID and PI-PI controllers given a settling time and control cycle are provided. They may be useful to obtain the settings quickly in practical applications. However, the design formulas can also be directly implemented using an IEC 61131-3 engineering software.

Lab experiments have confirmed the feasibility of the pole placement design. In particular, the smooth shape and settling time of the step responses have been verified both for continuous and discrete cases, as well as the ability of ramp tracking and disturbance suppression.

APPENDIX

Following notation from [11], let G denote a plant transfer function, $\widetilde{G}$ its approximation such that $\widetilde{G} = \widetilde{G}_+\widetilde{G}_-$ where $\widetilde{G}_+$ includes delays and right half-plane zeros, and has unity steady-state gain. To analyze the robustness of the approximation, an IMC controller R^* is defined

$$R^* = \frac{1}{\widetilde{G}_-} f, \tag{56}$$

where f denotes a low-pass filter that specifies a closed-loop transfer function (actually equal to $\widetilde{G}_+ f$). The controller R^* is designed for a feedback system involving $G - \widetilde{G}$ as a placeholder plant. It can be converted into the standard system with the original plant G and the controller R, where

$$R = \frac{R^*}{1 - R^*\widetilde{G}}. \tag{57}$$

In the case of the double integrator and perfect approximation we have $G = k_o/s^2 = \widetilde{G} = \widetilde{G}_-$ since $\widetilde{G}_+ = 1$. Taking into account integral action of the controller, assume the closed-loop transfer function as

$$f = \frac{as^2 + bs + 1}{(\lambda s + 1)^3}, \tag{58}$$

so with a triple time constant λ. Using (58) in (56), and then (56) in (57) gives

$$R = \frac{1}{k_o} \frac{s(as^2 + bs + 1)}{\lambda^3 s^2 + (3\lambda^2 - a)s + (3\lambda - b)}. \tag{59}$$

By taking $a = 3\lambda^2$ and $b = 3\lambda$ the controller R becomes of PID type, namely

$$R = \frac{3}{\lambda^2 k_o} + \frac{1}{\lambda^3 k_o}\frac{1}{s} + \frac{3}{\lambda k_o} s. \tag{60}$$

ACKNOWLEDGEMENTS

Discussions with Dr T. Żabiński and Prof. R. Leniowski are gratefully acknowledged.

REFERENCES

[1] B. Siciliano and O. Khatib, Eds., *Springer Handbook of Robotics*. Berlin Heidelberg: Springer, 2008.

[2] G. Ellis, Ed., *Control System Design Guide*, 4th ed. Butterworth-Heinemann, 2012.

[3] G.W. Younkin, *Industrial Servo Control Systems*, 2nd ed. New York: Marcel Dekker, 2002.

[4] S.-M. Yang and K.-W. Lin, "Automatic Control Loop Tuning for Permanent-Magnet AC Servo Motor Drives," *IEEE Trans. Ind. Electron.*, vol. 63, no. 3, pp. 1499–1506, 2016.

[5] G.F. Franklin, J.D. Powell, and A.F. Emami-Naeini, *Feedback Control of Dynamic Systems*, 7th ed. Reading: Addison-Wesley, 2019.

[6] L. Sciavicco and B. Siciliano, *Modelling and Control of Robot Manipulators*. London: Springer, 2000.

[7] T. Tarczewski, M. Skiwski, L.J. Niewiara, and L.M. Grzesiak, "High-performance PMSM servo-drive with constrained state feedback position controller," *Bull. Pol. Acad. Sci. Tech. Sci.*, vol. 66, pp. 49–58, 2018.

[8] V. Rao and D. Bernstein, "Naive control of the double integrator," *IEEE Control Syst. Mag.*, vol. 21, pp. 86–97, 2001.

[9] P.B. Schmidt and R.D. Lorenz, "Design principles and implementation of acceleration feedback to improve performance of DC drives," *IEEE Trans. Ind. Appl.*, vol. 28, no. 3, pp. 594–599, 1992.

[10] T. Żabiński and L. Trybus, "Tuning P-PI and PI-PI controllers for electrical servos," *Bull. Pol. Acad. Sci. Tech. Sci.*, vol. 58, pp. 51–58, 2010.

[11] D.E. Seborg, T.F. Edgar, D.A. Mellichamp, and F.J. Doyle, *Process Dynamics and Control*, 4th ed. New York: Wiley, 2016.

[12] C. Grimholt and S. Skogestad, "Optimal PI and PID control of first-order plus delay processes and evaluation of the original and improved SIMC rules," *J. Process Control*, vol. 70, pp. 36–46, 2018.

[13] K.J. Åström and T. Hägglund, *Advanced PID Control*, Research Triangle Park, 2005.

[14] "Maxima CAS homepage." [Online]. Available: https://maxima.sourceforge.io/.

[15] "ESTUN Industrial Technology Europe." [Online]. Available: https://www.estuneurope.eu/.

[16] "BECKHOFF New Automation Technology." [Online]. Available: https://www.beckhoff.com/.

[17] *EN 61131-3, Programmable controllers – Part 3: Programming languages (IEC 61131-3:2013), International Standard*, CENELEC Std., 2013.